Heat Mass Transfer (2005)
DOI 10.1007/s00231-005-0064-8

ORIGINAL

Abdalla M. Al-Amiri · Khalil Khanafer
Marilyn F. Lightstone

Unsteady numerical simulation of double diffusive convection heat transfer in a pulsating horizontal heating annulus

Received: 13 August 2004 / Accepted: 28 October 2005

Abstract A numerical study is conducted on time-dependent double-diffusive natural convection heat transfer in a horizontal annulus. The inner cylinder is heated with sinusoidally-varying temperature while the outer cylinder is maintained at a cold constant temperature. The numerical procedure used in the present work is based on the Galerkin weighted residual method of finite-element formulation by incorporating a non-uniform mesh size. Comparisons with previous studies are performed and the results show excellent agreement. In addition, the effects of pertinent dimensionless parameters such as the thermal Rayleigh number, Buoyancy ratio, Lewis number, and the amplitude of the thermal forcing on the flow and heat transfer characteristics are considered in the present study. Furthermore, the amplitude and frequency of the heated inner cylinder is found to cause significant augmentation in heat transfer rate. The predictions of the temporal variation of Nusselt and Sherwood numbers are obtained and discussed.

List of symbols

C'	Mass fraction (kg m^{-3})
C	Dimensionless concentration $= (C' - C'_o)/(C'_i - C'_o)$
D	Diffusion coefficient (m^2 s^{-1})
e_r, e_ϕ	Unit vectors in the radial and angular directions, respectively
f	Oscillating frequency (Hz)
g	Gravitational acceleration (ms^{-2})
Gr_C	Solutal Grashof number $= g\,\beta_C\,\Delta C'\,(r_o - r_i)^3/\nu^2$
Gr_T	Thermal Grashof number $= g\,\beta_T\,\Delta T\,(r_o - r_i)^3/\nu^2$
Le	Lewis number $= \alpha/D$
N	buoyancy ratio $= \beta_C \Delta C'/\beta_T \Delta T = Gr_C/Gr_T$
N_f	Brunt-Väisäla frequency $= \sqrt{g\beta\Delta T/(r_o - r_i)}$
$\overline{Nu}$	average Nusselt number
P	dimensionless pressure
Pr	Prandtl number $= \nu/\alpha$
r_i, r_o	radii of the inner and outer cylinders, respectively
R_i, R_o	dimensionless radii of the inner and outer cylinders, respectively
Ra	Rayleigh number $= g\,\beta\,\Delta T\,(r_o - r_i)^3/\nu\alpha$
Sc	Schmidt number $= \nu/D$
$\overline{Sh}$	Average Sherwood number
t	Time (s)
T	Temperature (K)
$\bar{T}$	Mean temperature (K)
u, v	Dimensionless velocity components in the radial and angular directions, respectively
u	velocity vector (ms^{-1})
x, y	Cartesian coordinates
X, Y	Dimensionless coordinates

Greek symbols

α	Thermal diffusivity (m^2 s^{-1})
β_T	Thermal expansion coefficient (m^3 kg^{-1})
β_C	Solutal expansion coefficient (K^{-1})
ΔT	Mean temperature difference between the inner and outer cylinders $= \overline{T_i} - T_o$
ε	Dimensionless amplitude of the temperature oscillation $= \Delta T'_i/\Delta T$

A. M. Al-Amiri
Mechanical Engineering Department, The United Arab Emirates University, P.O. Box 17555, Al-Ain, UAE
E-mail: alamiri@uaeu.ac.ae

K. Khanafer (✉)
Biomedical Engineering Department, University of Michigan, Ann Arbor, MI 48109, USA
E-mail: khanafer@umich.edu
Tel.: +1-734-7635240

M. F. Lightstone
Mechanical Engineering Department, McMaster University, Hamilton, ON L8S 4L7, Canada
E-mail: lightsm@mcmail.cis.mcmaster.ca

ϕ Angular coordinate
ν Kinematic viscosity ($m^2\ s^{-1}$)
λ Period of oscillation $= 2\pi/\varpi$
θ Dimensionless temperature $= (T - T_o)/(\bar{T}_i - T_o)$
ρ Density ($kg\ m^{-3}$)
ρ_∞ Density at reference temperature ($kg\ m^{-3}$)
τ Dimensionless time $= t\alpha\sqrt{Ra\,Pr}/(r_o - r_i)$
ϖ Dimensionless frequency of oscillation $= f/N_f$

Subscripts
i inner cylinder
o outer cylinder

1 Introduction

Natural convection heat transfer flow in enclosures with time periodic temperature boundary condition has received significant attention by many researchers [1–5]. This interest stems from its importance in many technological areas. Relevant examples include hazardous thermo-chemical spreading [6], fire protection techniques [7], building insulation [8], solar heating [9] and periodic energizing of electronic devices.

Numerical simulations and experiments have demonstrated that natural convection in an enclosure is intensified at certain discrete frequencies of the thermal boundary condition oscillation. This frequency is termed as resonance frequency and is characterized by achieving the maximum amplitude of heat transfer rate in the system. Lage and Bejan [10] illustrated the presence of resonance in natural convection inside an enclosure heated periodically from the side, where resonance was recognized from the maximum recorded amplitude of Nusselt number. In addition, Antohe and Lage [1, 5] extended the concept of resonance onto the transport process through porous media. Antohe and Lage [1] have numerically investigated heat and mass transport phenomena in a rectangular enclosure filled with a clear fluid and/or with fully saturated porous medium under time-periodic horizontal heating. Their results have indicated that the convection intensity within the enclosure increased linearly with heating amplitude for a wide range of parameters. Later on, Antohe and Lage [5] studied the effect of Prandtl number on the natural convection flow within an enclosure subjected to intermittent heating from the side. The authors have indicated in their study that natural convection resonance was smoothed, for the same Rayleigh number and Darcy number (in the case of a porous medium), when Prandtl number increased or decreased from a Prandtl number value of unity.

Resonant augmentation of natural convection for an incompressible fluid in a square enclosure having a constant cold sidewall temperature and an opposite sinusoidally varying hot sidewall temperature was studied numerically by Kwak et al. [9]. Their results revealed that a large amplitude wall temperature oscillation would cause an enhancement of the time-mean heat transfer rate. Furthermore, the maximum gain of the time-mean Nusselt number was found to occur at the resonance frequency. Chung et al. [3] numerically analyzed the effect of finite thickness and imperfect thermal conductivity of the boundary wall on buoyant convection in a square enclosure with a pulsating exterior surface temperature sustained at a high Rayleigh number. The finite-wall effect on the shift of resonance frequency was incorporated in this study. Experimental results of the natural convection generated by the time-periodic horizontal heating of a square cross-section enclosure were investigated by Antohe and Lage [11]. The reported heat transfer augmentation across an enclosure upon properly tuning the heating period. On the contrary, their results revealed that short heating periods hindered the convection within the enclosure.

Yang et al. [12] examined the effect of the sinusoidal time varying temperature oscillation of the hot and cold walls on natural convection in a tall vertical enclosure. The forcing frequency was fixed in their work while Rayleigh number values up to 10^6 were considered. What is more, Kazmierczak and Chinoda [13] analyzed the effect of frequency and amplitude of oscillating hot wall temperature on the flow and heat transfer in an enclosure. Xia et al. [14] examined the same problem configuration for high Rayleigh numbers and showed the impact of the wall temperature oscillation on the flow stability for a fixed value of frequency.

The problem of double diffusive convection has also been widely investigated in the past owing to the number of practical applications associated with this phenomenon such as crystal growth applied to semiconductors, melting and solidification processes in binary mixtures, storage of liquefied gases, and underground infiltration of pollutants. A thorough literature survey revealed that most of the studies associated with annulus configurations were focused on the analysis of thermal convection. In contrast, the majority of the investigations dealing with double diffusive natural convection were found to be restricted to rectangular enclosures. Shipp et al. [15, 16] conducted a numerical study for steady laminar double-diffusive natural convection within a vertical closed annulus with constant temperature and mass species differences imposed across the vertical walls. The effect of buoyancy ratio on the flow structure and the resulting heat and mass transfer rates was illustrated in their work. Recently, Khanafer et al. [17] analyzed numerically water diffusion within the brain tissue for various clinical conditions. A wide range of pertinent parameters such as Lewis number, cell volume, and the buoyancy ratio were considered in their study. The results showed that

the diffusion coefficient, cell volume, and the buoyancy ratio play significant roles on the characterization of the mass and heat transfer mechanisms within the cell. Experimental tests were also conducted to produce an 8-T image, which was compared with their numerical simulation. Later on, the same authors conducted a numerical study [18] on the diffusion process within the structure of a brain extracellular space for various diffusion parameters of brain tissue namely extracellular space porosity and tortuosity. The results obtained seem to play an important role in producing more effective imaging techniques for brain injury based on the apparent diffusion coefficient.

To the best knowledge of the present authors, no attention has given to double diffusive convection heat transfer in a pulsating horizontal heating annulus. The aim of the present investigation is to depict numerically the time-dependent buoyant convection in an annulus subject to a periodically varying temperature condition imposed on the inner cylinder of the annulus. The effects of pertinent parameters such as the thermal forcing amplitude and frequency, Lewis number, thermal Rayleigh number, and buoyancy ratio on the flow and heat and mass transfer characteristics were considered in the present study.

2 Problem formulation

Consider unsteady double diffusive natural convection in a horizontally oriented two concentric cylinders. The geometry of the problem and the coordinate system are shown in Fig. 1. The working fluid within the annulus is assumed to be Newtonian, incompressible, and laminar with a Prandtl number of $Pr = 0.7$. The inner cylinder of radius r_i is kept at a relatively higher temperature and concentration $[T_i = \bar{T}_i + \Delta T'_i \sin(f\,t)$ and $C'_i]$ while the outer cylinder of radius r_o is kept at lower temperature and concentration (T_o and C'_o). Here, f and t represent the frequency of the inner cylinder temperature oscillation and elapsed time. The physical geometry of the annulus was fixed by setting the inner and outer radii to 1.0 and 2.6, respectively. The thermophysical properties of the fluid are assumed to be constant except the density

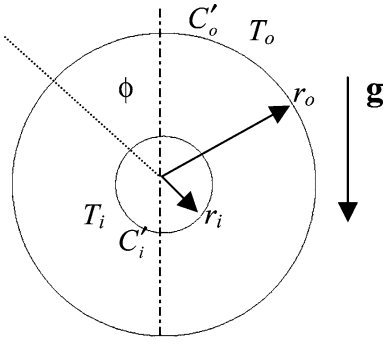

Fig. 1 Schematic of the physical model and coordinate system

variation in the buoyancy force, which is treated according to the Boussinesq approximation. This variation, due to both temperature and concentration gradients, can be described by the following equation

$$\rho = \rho_\infty \left[1 - \beta_T (T - T_o) - \beta_C (C' - C'_o)\right] \tag{1}$$

where β_T and β_C are the coefficients for thermal and concentration expansions, respectively, such that

$$\beta_T = -\frac{1}{\rho_\infty}\left(\frac{\partial \rho}{\partial T}\right)_{P,C'}, \quad \beta_C = -\frac{1}{\rho_\infty}\left(\frac{\partial \rho}{\partial C'}\right)_{P,T} \tag{2}$$

To render the equations non-dimensional, the following dimensionless parameters are introduced

$$R_i = \frac{r_i}{(r_o - r_i)}, \quad R_o = \frac{r_o}{(r_o - r_i)}, \quad \mathbf{u} = \frac{(u, v)\,(r_o - r_i)}{\alpha\sqrt{Ra\,Pr}}, \quad \tau = \frac{t\alpha\sqrt{Ra\,Pr}}{(r_o - r_i)^2}$$

$$\theta = \frac{T - T_o}{\bar{T}_i - T_o}, \quad C = \frac{C' - C'_o}{C'_i - C'_o}, \quad P = \frac{p(r_o - r_i)^2}{\rho\alpha^2 Ra\,Pr} \tag{3}$$

The dimensionless amplitude of thermal forcing is $\varepsilon = \Delta T'_i / \Delta T$ while the dimensionless frequency is given by $\varpi = f/N_f$. Here, N_f is the Brunt-Väisäla frequency, which is equal to $N_f = \sqrt{g\beta_T \Delta T/(r_o - r_i)}$. Therefore, the non-dimensional governing equations can be written as

$$\nabla \cdot \mathbf{u} = 0 \tag{4}$$

$$\frac{\partial \mathbf{u}}{\partial \tau} + (\mathbf{u} \cdot \nabla)\,\mathbf{u} = -\nabla P + \frac{\nabla^2 \mathbf{u}}{\sqrt{Gr_T}} + \left((\theta + NC)\cos\phi\, e_r - (\theta + NC)\sin\phi\, e_\phi\right) \tag{5}$$

$$\frac{\partial \theta}{\partial \tau} + (\mathbf{u} \cdot \nabla)\,\theta = \frac{\nabla^2 \theta}{Pr\sqrt{Gr_T}} \tag{6}$$

$$\frac{\partial C}{\partial \tau} + (\mathbf{u} \cdot \nabla)\,C = \frac{\nabla^2 C}{Sc\sqrt{Gr_T}} \tag{7}$$

where $\mathbf{u}$ is the velocity vector (u,v) and N is buoyancy ratio given by $N = \beta_C\,\Delta C / \beta_T\,\Delta T = Gr_C/Gr_T$. The non-dimensional parameters in the above equations are the Grashof number $Gr_T = g\beta_T(\bar{T}_i - T_o)\,(r_o - r_i)^3/\nu^2$, the solutal Grashof number $Gr_C = g\beta_C(C'_i - C'_o)\,(r_o - r_i)^3/\nu^2$, and Schmidt number $Sc = \nu\,/D$, respectively. In these equations, the following dimensionless variables α, D, and ν are the thermal diffusivity, diffusion coefficient, and the kinematic viscosity of the fluid, respectively. It is worth mentioning that a negative buoyancy ratio (N) value reflects a negative solutal expansion coefficient in the considered temperature range.

A steady state solution corresponding to the non-oscillating case ($\varepsilon = 0$) was used as an initial condition in simulating the cases of time-varying temperature

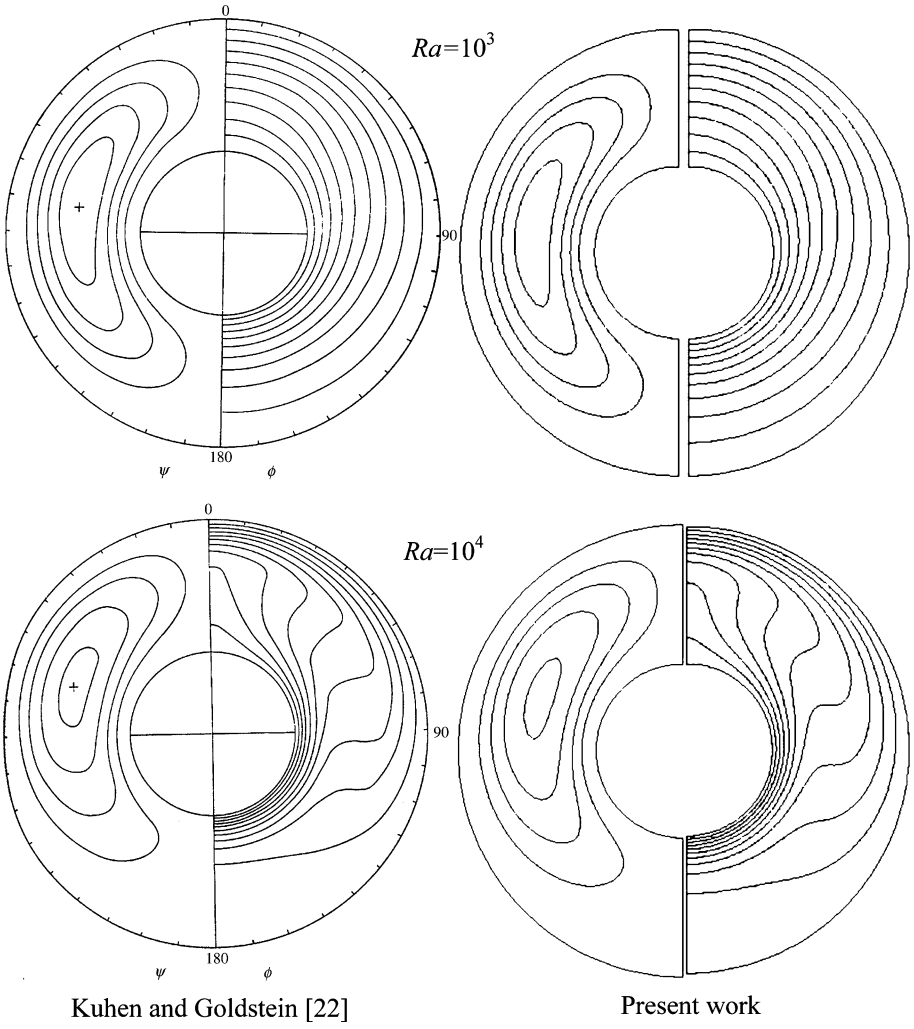

Fig. 2 Comparison of streamlines and isotherms for the 2-D annulus

conditions. The boundary conditions for the problem under consideration are expressed as:

$$u = \mathrm{v} = 0, C = 1, \theta = 1 + \varepsilon \sin(\varpi\tau) \quad \text{at } R_\mathrm{i} \tag{8}$$

$$u = \mathrm{v} = 0, C = \theta = 0 \quad \text{at } R_\mathrm{o} \tag{9}$$

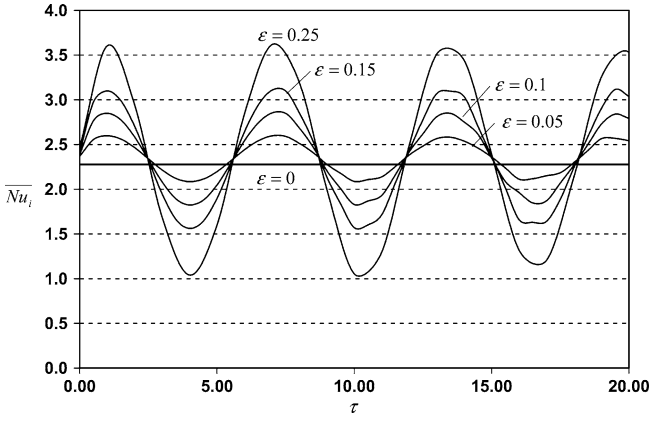

Fig. 3 Temporal variation of the inner cylinder average Nusselt number against the dimensionless temperature amplitude ($Ra = 10^4$, $Le = 1$, $N = 1$, $\varpi = 1$)

The local Nusselt number distributions along the inner and outer cylinders are calculated as the actual heat transfer divided by the heat transfer for pure conduction in the absence of fluid motion as follows

$$Nu_\mathrm{i}(\phi) = \frac{Q_\mathrm{i}}{Q_\mathrm{cond}} = -\frac{(2\pi RLk)(\partial\theta/\partial R)_{R=R_\mathrm{i}}}{1/(2\pi Lk\ln(R_\mathrm{o}/R_\mathrm{i}))} = -\ln(\frac{R_\mathrm{o}}{R_\mathrm{i}})\left(R\frac{\partial\theta}{\partial R}\right)_{R=R_\mathrm{i}} \tag{10}$$

$$Nu_\mathrm{o}(\phi) = \frac{Q_\mathrm{o}}{Q_\mathrm{cond}} = -\frac{(2\pi RLk)(\partial\theta/\partial R)_{R=R_\mathrm{o}}}{1/(2\pi Lk\ln R_\mathrm{o}/R_\mathrm{i})} = -\ln\frac{R_\mathrm{o}}{R_\mathrm{i}}\left(R\frac{\partial\theta}{\partial R}\right)_{R=R_\mathrm{o}} \tag{11}$$

Meanwhile, the average Nusselt numbers estimated at the inner and outer cylinders are given by

$$\overline{Nu}_\mathrm{i} = \frac{1}{2\pi}\int_0^{2\pi} Nu_\mathrm{i}(\phi)\,\mathrm{d}\phi \quad \&38; \quad \overline{Nu}_\mathrm{o} = \frac{1}{2\pi}\int_0^{2\pi} Nu_\mathrm{o}(\phi)\,\mathrm{d}\phi \tag{12}$$

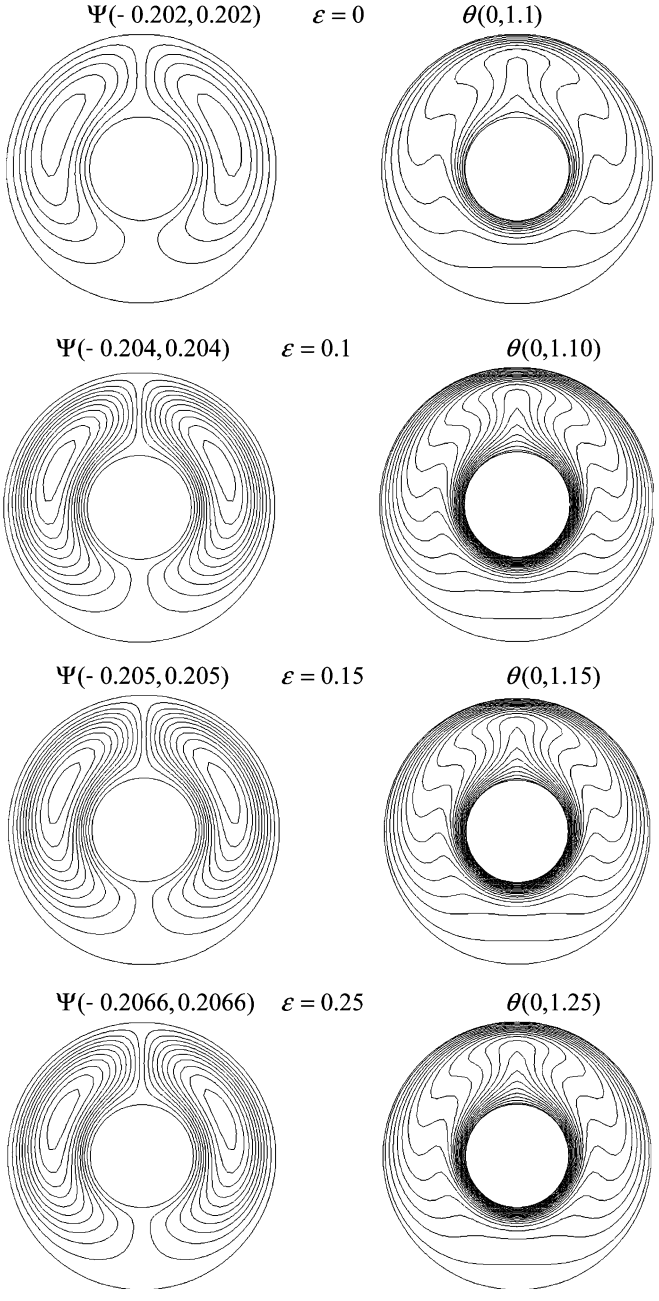

Fig. 4 Effect of the amplitude of the hot inner cylinder temperature oscillation on the streamlines and isotherms ($Ra = 10^4$, $Le = 1$, $N = 1$, $\varpi = 1, \lambda = 0.25\,(2\pi/\varpi)$)

Under steady state conditions, both expressions in Eq. (12) should converge to the same results. Similarly, the average Sherwood numbers at the inner and outer cylinders are obtained as follows

$$\overline{Sh}_{\mathrm{i}} = \frac{1}{2\pi}\int_0^{2\pi} Sh_{\mathrm{i}}(\phi)\mathrm{d}\phi \quad \& \quad \overline{Sh}_{\mathrm{o}} = \frac{1}{2\pi}\int_0^{2\pi} Sh_{\mathrm{o}}(\phi)\mathrm{d}\phi \qquad (13)$$

where

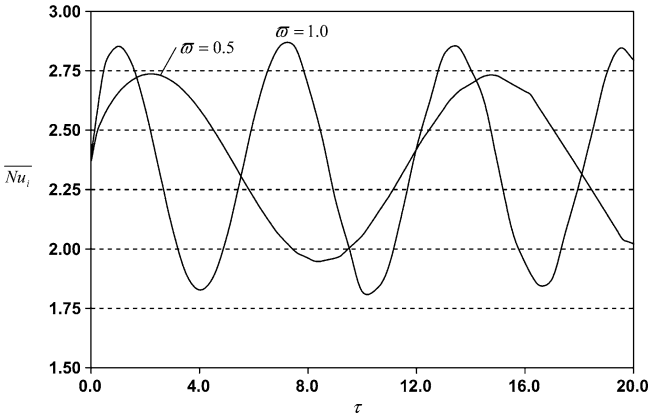

Fig. 5 Temporal variation of the inner cylinder average Nusselt number against the dimensionless temperature frequency ($Ra = 10^4$, $Le = 1$, $N = 1$, $\varepsilon = 0.1$)

$$Sh_{\mathrm{i}}(\phi) = -\ln\frac{R_{\mathrm{o}}}{R_{\mathrm{i}}}\left(R\frac{\partial C}{\partial R}\right)_{R=R_{\mathrm{i}}}$$
$$Sh_{\mathrm{o}}(\phi) = -\ln\frac{R_{\mathrm{o}}}{R_{\mathrm{i}}}\left(R\frac{\partial C}{\partial R}\right)_{R=R_{\mathrm{o}}} \qquad (14)$$

3 Numerical scheme

A finite element formulation based on the Galerkin method is employed to solve the governing equations subject to the initial and boundary conditions for the present study. The application of this technique is well described by Taylor and Hood [19] and Gresho et al. [20], and its application is well documented [21]. The highly coupled and non-linear algebraic set of equations, which are obtained from the discretization of the governing equations, is solved using an iterative solution scheme, namely the segregated solution algorithm. The advantage of using this method is that the global system matrix is decomposed into smaller submatrices and then solved in a sequential manner. In essence, this technique results in considerably fewer storage requirements. Furthermore, the conjugate residual scheme is used to solve the symmetric pressure-type equation systems, while the conjugate gradient squared method is used for the non-symmetric advection–diffusion-type equations. The present numerical approach was verified against the published results by Kuhen and Goldstein [22] for thermal natural convection within the annulus as shown in Fig. 2. It can be seen from the figure that both solutions are in excellent agreement.

4 Results and discussion

The analyses in the undergoing numerical investigation are performed in the following domain of the associated dimensionless groups: $0 \leqslant \varepsilon \leqslant 0.25$, $0.5 \leqslant \varpi \leqslant 1.0$, $10^3 \leqslant$

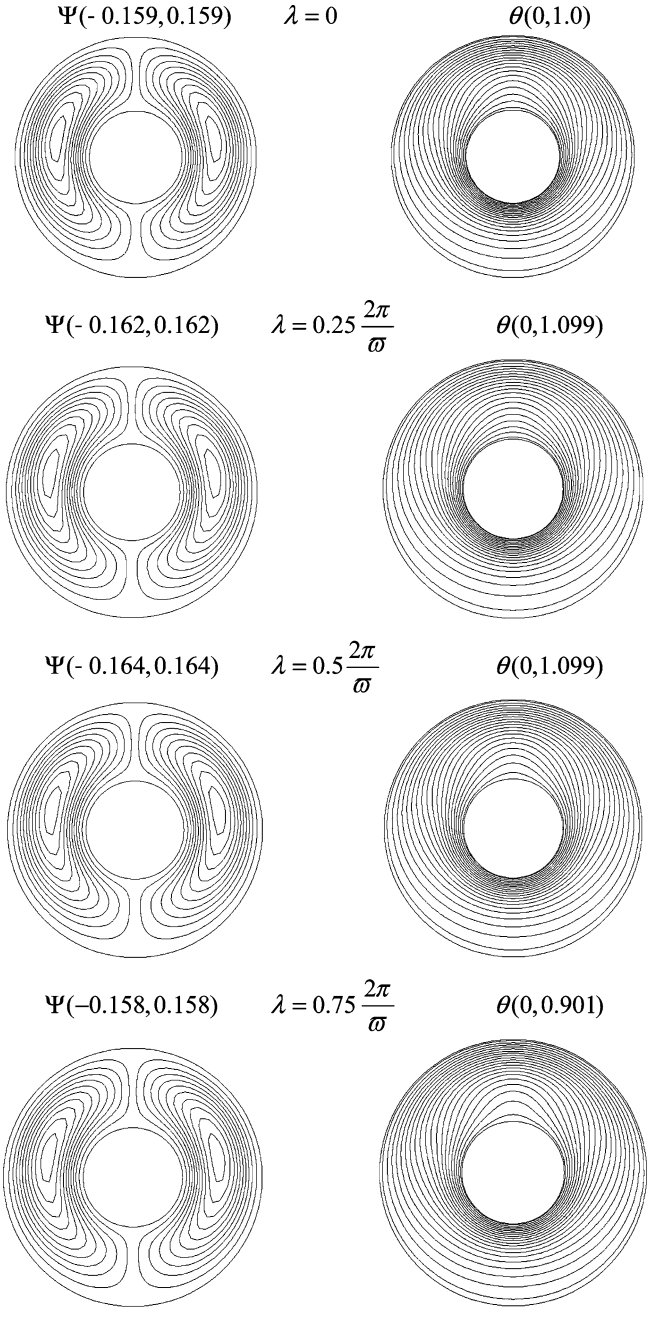

Fig. 6 Temporal variation of the streamlines and isotherms ($Ra = 10^3$, $Pr = 0.7$, $Le = 1$, $N = 1$, $\varepsilon = 0.1$, $\varpi = 1$)

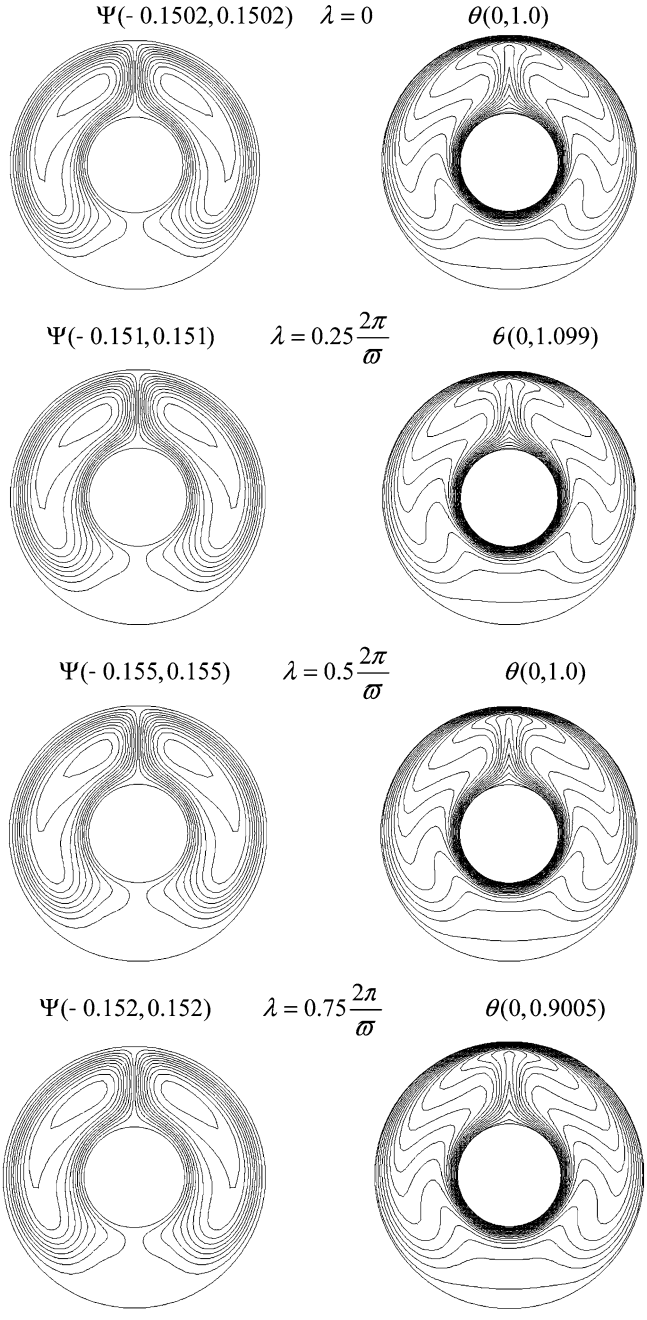

Fig. 7 Temporal variation of the streamlines and isotherms ($Ra = 5 \times 10^4$, $Pr = 0.7$, $Le = 1$, $N = 1$, $\varepsilon = 0.1$, $\varpi = 1$)

$Ra \leqslant 5 \times 10^4$, $0.1 \leqslant Le \leqslant 5$ and $-1 \leqslant N \leqslant 5$. The default case study carried the following dimensionless group values: $\varepsilon = 0.1$, $\varpi = 1.0$, $Ra = 10^4$, $Le = 1$, and $N = 1$. The results are presented in terms of the contour lines for the streamline, temperature, and concentration. In addition, the temporal Nusselt number, average Nusselt number and Sherwood number predictions are also presented.

The effect of the amplitude of the high temperature inner cylinder oscillation on the temporal variation of the average Nusselt number along the inner cylinder is shown in Fig. 3. The average Nusselt number along the inner cylinder appears to fluctuate periodically by the sinusoidal oscillation of the inner cylinder. As the amplitude of forcing ε increases, the temporal variation of the average Nusselt number is augmented. This is attributed to the fact that the inner cylinder temperature oscillates notably with large amplitude values. Hence, natural convection heat transfer within the annulus intensifies since the thickness of the thermal boundary layer decreases along the inner cylinder with an increase in ε value. This is evident in Fig. 4, which illustrates the effect of varying the forcing amplitude ε on the temperature and flow structures within the annulus for a

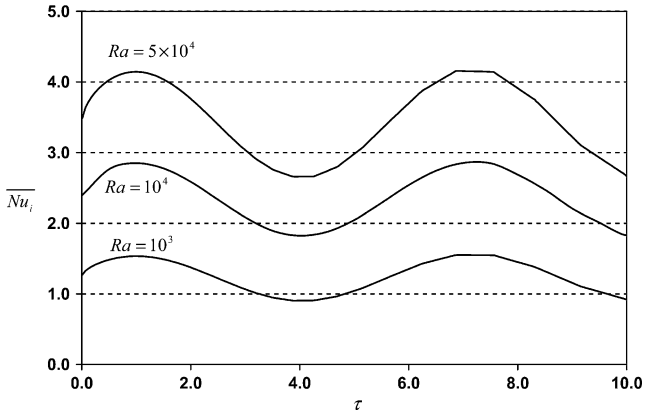

Fig. 8 Temporal variation of the inner cylinder average Nusselt number using various Rayleigh number values ($Le = 1$, $N = 1$, $\varepsilon = 0.1$, $\varpi = 1$)

specific period of time. This figure also shows that the intensity of velocity circulation within the annulus increases which results in higher heat transfer rate. The maximum and minimum values of the streamlines are documented for the considered ε values.

The effect of varying the dimensionless frequency ϖ on the temporal variation of the average Nusselt number computed at the inner cylinder is presented in Fig. 5. This figure depicts that the temporal behavior of the average Nusselt number reaches a quasi-steady periodic form after several periodical cycles. Apparently, the fluctuating amplitude of the average Nusselt number becomes substantially larger at elevated dimensionless frequency values as illustrated in Fig. 5. This signals that the heat transfer rate within the annulus enhances with an increase in ϖ value.

Temporal variation of the streamlines and isotherms for Rayleigh numbers of 10^3 and 5×10^4 is shown in Figs. 6 and 7, respectively. The results, which are displayed for different oscillation periods (λ), clearly reflect the significant impact of the Rayeligh number on the structure of the streamlines and isotherms within the annulus for various time periods. For a Rayleigh number value of 10^3, heat transfer within the annulus is primarily communicated by conduction mechanism as displayed in Fig. 6. As the Rayleigh number increase to 5×10^4, however, heat transfer within the annulus enhances significantly as shown in Fig. 7. The onset of the thermal convection currents brings about the formation

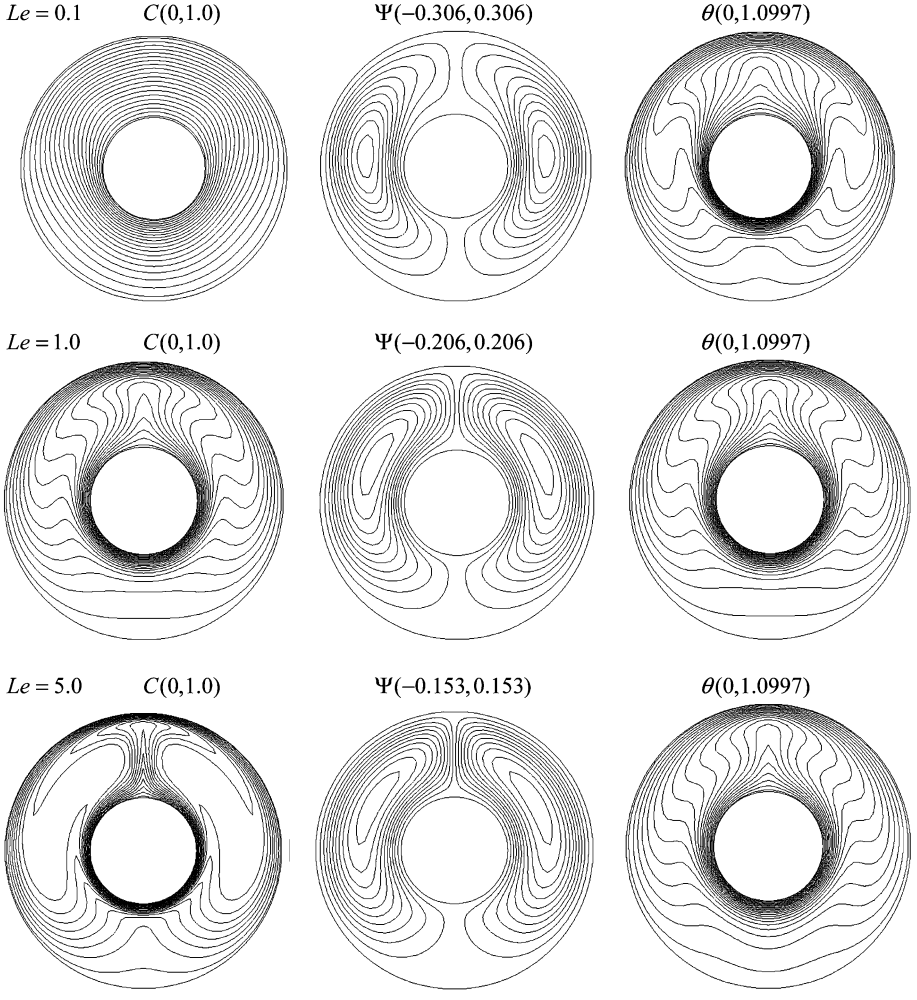

Fig. 9 Effect of Lewis number on the streamlines and isotherms ($Ra = 10^4$, $N = 1$, $\varepsilon = 0.1$, $\lambda = 0.25\,(2\pi/\varpi)$, $\varpi = 1.0$)

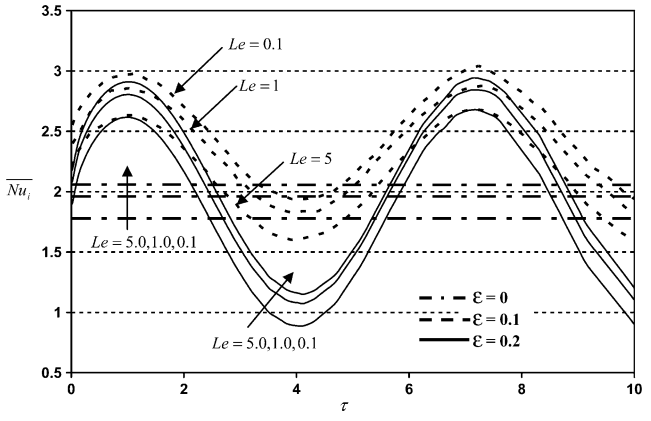

Fig. 10 Temporal variation of the inner cylinder average Nusselt number using various dimensionless amplitude of the temperature oscillation and Lewis number values ($Ra = 10^4$, $N = 1$, $\varpi = 1.0$)

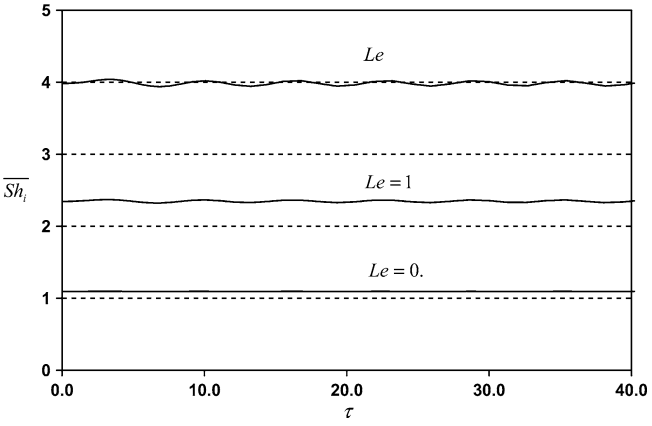

Fig. 11 Temporal variation of the inner cylinder average Sherwood number for using various Lewis number values ($Ra = 10^4$, $N = 1$, $\varepsilon = 0.1$, $\varpi = 1.0$)

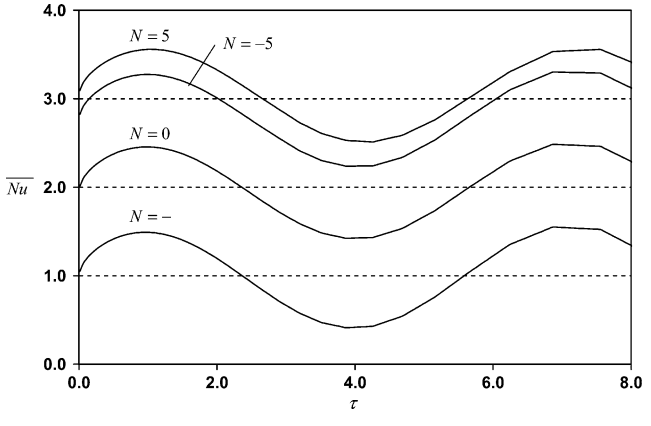

Fig. 12 Effect of the Buoyancy ratio on the temporal variation of the inner cylinder average Nusselt number ($Ra = 10^4$, $Le = 1$, $\varepsilon = 0.1$, $\varpi = 1.0$)

of thinner boundary layer along the inner cylinder. It is vivid from the results that conduction heat transfer is overwhelmed by high natural convection currents. A further insight into the influence of Rayleigh number is achieved by examining its impact on the temporal variation of the inner cylinder average Nusselt number ($\overline{Nu}_i$). As can be seen from Fig. 8, heat transfer within the annulus is dominated by conduction mechanism when considering low Rayleigh number values. This is manifested by the swing of $\overline{Nu}_i$ predictions around unity. As the Rayleigh number increases, the intensity of the natural convection within the annulus increases, which subsequently augments $\overline{Nu}_i$ predictions. For instance, the heat transfer has improved by 92% as Rayleigh number increased from 10^3 to 10^4. Such improvement is noticed to reach 180% as Rayleigh number increased from 10^3 to 5×10^4.

Next, the effect of the Lewis number is evaluated through the presentation of the isoconcentration contours, streamlines, and isotherms as illustrated in Fig. 9. It can be seen in this figure that for a low Lewis number of $Le = 0.1$, mass transport within the annulus is chiefly controlled by the diffusion process. As the Lewis number increases, however, a significant change occurs in the concentration contours due to the formation of thinner mass boundary layers in the vicinity of the inner cylinder as displayed in Fig. 9. This translates into sharp concentration gradients that improve the mass transfer rate within the annulus. The effect of Lewis number on streamlines and isotherms is also documented in Fig. 9. The results show that the increase in Lewis number brings about a reduction in the intensity of flow circulation within the annulus due to thickening in the formed thermal boundary layers. This can be clearly observed from the distribution of isotherms in Fig. 9.

The effect of Lewis number on the dimensionless heat (average Nusselt number) and dimensionless mass (average Sherwood number) transfer rates is shown in Figs. 10 and 11, respectively. Figure 10 shows the temporal variation of the average Nusselt number at the inner cylinder for various Lewis numbers and dimensionless amplitude of the temperature oscillation. The temporal variation of inner cylinder average Nusselt number is constant for zero amplitude of the temperature oscillation. Figure 10 illustrates that the temporal variation of the inner cylinder average Nusselt number is higher for $\varepsilon = 0.1$ than in case of $\varepsilon = 0.2$. The increase in Lewis number brings about thickening of the thermal boundary layer, which causes depreciation in the heat transfer rate within the annulus. On the contrary, the increase in Lewis number appears to suppress the solutal boundary layer, which results in mass transfer enhancement within the annulus as depicted in Fig. 11. As such, the average Sherwood number increased is denoted to by 250% as the Lewis number increased from 0.1 to 5. Figure 11 also shows that for the low Lewis number of $Le = 0.1$, mass transfer within the annulus is mainly achieved by a diffusion process. When a high Lewis number is considered, such as $Le = 5$, mass

transfer rate within the annulus seems to increase and Sherwood number predictions exhibit an oscillating pattern as shown in the figure.

Finally, the effect of the buoyancy ratio (N) on the temporal variation of the average Nusselt number along the inner cylinder is presented in Fig. 12. In essence, the buoyancy ratio is a measure of the concentration potential to that achieved by thermal convection. It can be seen in Fig. 12 that for the buoyancy ratio of $N=-1$, the thermal buoyancy forces due to the heating of the inner cylinder and the solutal buoyancy forces are equal in magnitude but act in opposing direction such that they nullify each other presence. Thus, the transport process within the annulus becomes entirely dominated by the diffusion process. This is clearly illustrated in Fig. 12 as the $\overline{Nu}_i$ predicted values swing around unity. As the buoyancy ratio increases, the thermal and solutal boundary layers become thinner along the inner surface of the annulus. This consequently result in higher temperature and concentration gradients in the direction normal to the surface, which translates into higher heat and mass transfer rates within the annulus. As a result, the flow circulation within the annulus is substantially augmented. When a high buoyancy ratio number is considered such as $N=5$ (aiding flow scenario), the diffusion process is apparently replaced by the combined convective thermosolutal phenomenon. This is also true when $N=-5$ (opposing flow scenario) as shown in Fig. 12.

5 Conclusions

Numerical simulations have been carried out for double diffusive convection heat transfer in a horizontally-oriented annulus. The inner cylinder is considered to be heated in a pulsating manner. The effects of amplitude and frequency of the heated inner cylinder on the temporal variation of the average Nusselt number are investigated. In addition, physical insight into the mass and energy transport mechanisms was provided based on a number of pertinent dimensionless parameters. The results of the present investigation illustrate that augmentation of heat transfer can be achieved by increasing the thermal forcing amplitude and/or frequency, increase of thermal Rayleigh number. Furthermore, high heat transfer can be attained within the annulus upon decreasing the Lewis number and increasing the buoyancy ratio parameter. What is more, the results show that the increase in the Lewis number brings about an appreciated increase in mass transfer within the annulus due to the increase in the mass diffusion as compared to thermal diffusion.

Acknowledgments The first author is grateful to the UAE University Research Council for its generous grant under contract number 02-05-7-11/03 while the two latter authors expresses their appreciation for the grant received from National Sciences and Engineering Research Council of Canada (*NSERC*-2002) in support of this investigation.

References

1. Antohe B, Lage J (1996) Amplitude effect on convection induced by time-periodic horizontal heating. Int J Heat Mass Transfer 38:1121–1133
2. Lee C, Hyun J, Kwak H (2000) Oscillatory enclosed buoyant convection of a fluid with the density maximum. Int J Heat Mass Transfer 43:3747–3751
3. Chung K, Kwak H, Hyun J (2001) Finite-wall effect on buoyant convection in an enclosure with pulsating exterior surface temperature. Int J Heat Mass Transfer 44:721–732
4. Kim K, Hyun J, Kwak H (2001) Buoyant convection in a side-heated cavity under gravity and oscillations. Int J Heat Mass Transfer 44:857–861
5. Antohe B, Lage J (1997) The Prandtl number effect on the optimum heating frequency of an enclosure filled with fluid or with a saturated porous medium. Int J Heat Mass Transfer 40:1313–1323
6. Zhang Z, Bejan A (1987) The horizontal spreading of thermal and chemical deposits in a porous medium. Int J Heat Mass Transfer 30:2289–2303
7. Yano T, Ochi M, Enya S (1990) Protection against fire and high temperature by using porous media and water. Proc ASME/JSME Thermal Eng Conf 4:213–218
8. Wijeysundera NE, Hawlader MNA (1992) Effects of condensation and liquid transport on thermal performance of fibrous insulations. Int J Heat Mass Transfer 35:2605–2616
9. Kwak H, Kuwahara K, Hyun J (1998) Resonant enhancement of natural convection heat transfer in a square enclosure. Int J Heat Mass Transfer 41:2837–2846
10. Lage J, Bejan A (1993) The resonance of natural convection in an enclosure heated periodically from the side. Int J Heat Mass Transfer 36:2027–2038
11. Antohe B, Lage J (1996) Experimental investigation on pulsating horizontal heating of a water-filled enclosure. ASME J Heat Transfer 118:889–896
12. Yang HT, Yang KT, Xia Q (1989) Periodic laminar convection in a tall vertical cavity. Int J Heat Mass Transfer 32:2199–2207
13. Kazmierczak M, Chinoda Z (1992) Buoyancy driven flow in an enclosure with time periodic conditions. Int J Heat Mass Transfer 35:1507–1518
14. Xia Q, Yang KT, Mukutomi D (1995) Effects of imposed wall temperature oscillations on the stability of natural convection in a square enclosure. ASME J Heat Transfer 117:113–120
15. Shipp PW, Shoukri M, Carver MB (1993) Double diffusive natural convection in a closed annulus. Num Heat Transfer Part A 24:339–356
16. Shipp PW, Shoukri M, Carver MB (1993) Effect of thermal Rayleigh and Lewis numbers on double diffusive natural convection in closed annulus. Num Heat Transfer Part A 24:451–465
17. Khanafer K, Vafai K, Kangarlu A (2003) Water diffusion in biomedical systems as related to magnetic resonance imaging. Magn Reson Imaging 21:17–31
18. Khanafer K, Vafai K, Kangarlu A (2003) Computational modeling of cerebral diffusion-application to stroke imaging. Magn Reson Imaging 21:651–661
19. Taylor C, Hood P (1973) A numerical solution of the navier–stokes equations using finite-element technique. Comput Fluids 1:73–89
20. Gresho PM, Lee RL, Sani RL (1980) On the time-dependent solution of the incompressible Navier–Stokes equations in two and three dimensions recent advances in numerical methods in fluids. Pineridge, Swansea
21. FIDAP (1990) Theoretical manual. Fluid dynamics international. Evanston, ILL
22. Kuhen TH, Goldstein RJ (1976) An experimental and theoretical study of natural convection in the annulus between horizontal concentric cylinders. J Fluid Mech 74:695–719